

Journal of Materials Chemistry A

Accepted Manuscript



This is an *Accepted Manuscript*, which has been through the Royal Society of Chemistry peer review process and has been accepted for publication.

Accepted Manuscripts are published online shortly after acceptance, before technical editing, formatting and proof reading. Using this free service, authors can make their results available to the community, in citable form, before we publish the edited article. We will replace this *Accepted Manuscript* with the edited and formatted *Advance Article* as soon as it is available.

You can find more information about *Accepted Manuscripts* in the [Information for Authors](#).

Please note that technical editing may introduce minor changes to the text and/or graphics, which may alter content. The journal's standard [Terms & Conditions](#) and the [Ethical guidelines](#) still apply. In no event shall the Royal Society of Chemistry be held responsible for any errors or omissions in this *Accepted Manuscript* or any consequences arising from the use of any information it contains.

Cite this: DOI: 10.1039/c0xx00000x

www.rsc.org/xxxxxx

ARTICLE TYPE

Multifunctional and Robust Covalent Organic Framework-Nanoparticles Hybrids

Pradip Pachfule,^a Manas K. Panda,^a Sharath Kandambeth,^a S. M. Shivaprasad,^b David Díaz Díaz,^c and Rahul Banerjee^{a*}

Received (in XXX, XXX) Xth XXXXXXXXX 20XX, Accepted Xth XXXXXXXXX 20XX
DOI: 10.1039/b000000x

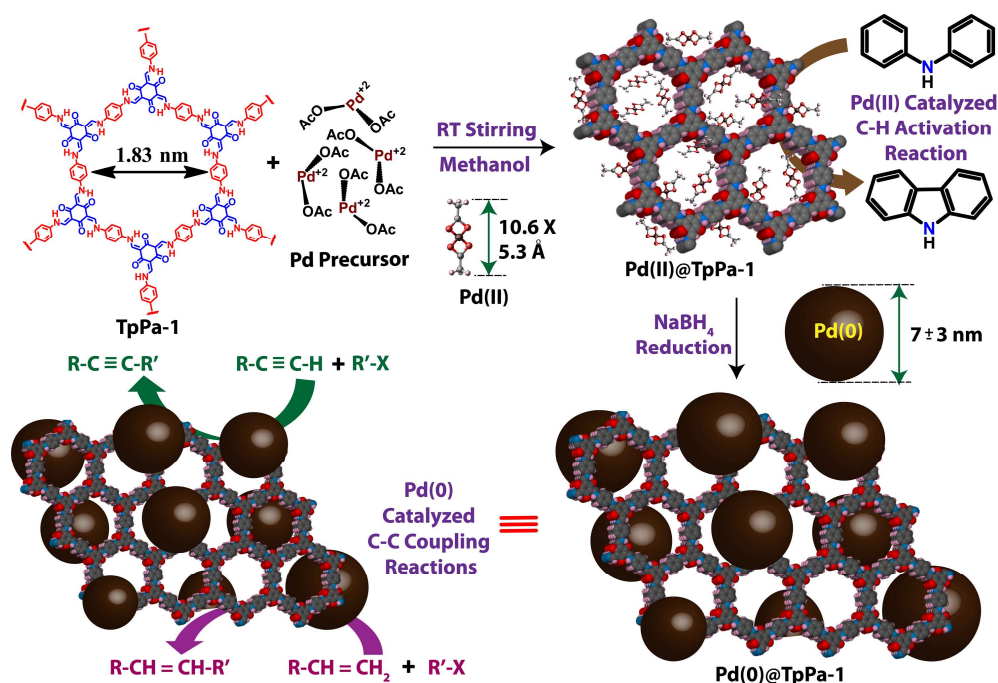
Highly dispersed Pd(0) nanoparticles were successfully immobilized in a stable, crystalline and porous covalent organic framework (COF), **TpPa-1**, by a solution infiltration method using NaBH_4 as reducing agent. High resolution and dark field TEM images confirmed the uniform loading of the Pd(0) nanoparticles into the **TpPa-1** matrix without aggregation. This hybrid material exhibited excellent catalytic activity towards the Cu free Sonogashira, Heck and sequential one pot Heck/Sonogashira cross coupling reactions under basic conditions, and with superior performance than commercially available Pd supported on activated charcoal (i.e., 1, 5 and 10 wt.%). Additionally, the precursor Pd(II)-doped COF also displayed competitive catalytic activity for the intramolecular oxidative biaryl synthesis under acidic conditions. Both catalysts were found to be highly stable under the reaction conditions showing negligible metal leaching, non-sintering behavior, and good recyclability. To the best of our knowledge, the organic support used in this work, **TpPa-1**, constitutes the first COF matrix that can hold both Pd(0) nanoparticles and Pd(II) complex without aggregation for catalytic purposes under both highly acidic and basic conditions.

Introduction

Covalent organic frameworks (COFs) are porous and crystalline solids synthesized by extending organic structures via strong covalent bonds are well known for its applications in gas storage, catalytic supports, semiconductive and photoconductive devices.¹ The availability of confined space for nucleation with high surface area, porosity, chemical tunability and structural regularity present in COFs supports a reasonable choice of these materials as versatile supports for various catalytically active nanoparticles.² Additionally due to the in-built covalent bond architecture, one could anticipate that COFs might become more suitable scaffolds than that of metal organic frameworks (MOFs) for anchoring metal nanoparticles and therefore emerge as versatile and efficient organic supports for heterogeneous catalysis.³ Indeed, such MOF and COF derived hybrids has been used as catalysts in diverse reactions such as Suzuki coupling,^{2c,2f} C–H activation,^{3e} nitro reduction,^{3f} and glycerol oxidation reactions, etc.^{2b} However, a major limitation of these materials to act as porous hosts is their moderate stability under standard experimental conditions in aqueous, acidic and basic media.⁴ This creates the necessity for the development of improved heterogeneous supports for holding catalytically active nanoparticles. Unfortunately, due to the deficient stability of these frameworks, the loading of metal nanoparticles have mainly been performed by tedious routes like chemical vapor deposition, solid grinding and solution infiltration followed by H_2/He stream reduction.^{2–4} The treatment of COF supports after metal loading with reducing agents like, for example, NaBH_4 , LiAlH_4 or

hydrazine has been avoided to maintain the framework rigidity and crystallinity of the supports. The loss of crystallinity and rigidity of these COF supports due to the spontaneous treatment with reducing agents further leads to the decreased interaction between support and nanoparticles. This results into the leaching and sintering of nanoparticles, which is a major reason for loss of catalytic activity during repeated cycles.^{3d,3i} Also, the utilization of these nanoparticles@MOFs/COFs as a catalyst towards the reactions, to be performed in aqueous/acidic/basic medium has been avoided. To the best of our knowledge, there exists an example containing Pd(II) on crystalline COF that exhibited catalytic activity for Suzuki coupling reactions.^{2c} Also, the incorporation of Pd and Pt nanoparticles into amorphous covalent triazine frameworks (CTFs) for glycerol, alcohol and methane oxidation has been reported.^{2a,2b,2e} Moreover, the utilization of chemically unstable COF-102 for the immobilization of Pd(0) nanoparticles and volatile organometallic precursor for room temperature (RT) hydrogen uptake and catalysis has been described elsewhere.^{2d,2g} It is noteworthy that, most of the aforementioned COFs are either amorphous or unstable to the reaction conditions performed in aqueous, acidic or basic media.²

In the area of organic synthesis and catalysis, transition metal catalyzed C–C coupling and C–H activation reactions constitute a powerful tool.^{5,6} Among the transition metals palladium poses one of the strongest tendencies to form bonds with carbon,⁷ which has motivated scientists over the last decades to develop and optimize these catalytic processes to a stage that has enabled application on an industrial scale. In addition, the



Scheme 1. Synthesis of Pd(II) and Pd(0)-doped COFs (i.e., **Pd(II)@TpPa-1**, **Pd(0)@TpPa-1**) and summary of their catalytic activity towards Sonogashira, Heck and oxidative biaryl couplings. The doped Pd(0) nanoparticles are probably situated on TpPa-1 surface. [The scheme is to represent the synthesis and the organization of the Pd nanoparticles on COF (TpPa-1) and it is not exactly fit to scale].

heterogenization (or immobilization) of transition metal catalysts has been also receiving considerable attention, as these hybrids combine the advantages of both the homogeneous and heterogeneous catalyst within the context of green chemistry and sustainable design.⁸ In this regard, along with charcoal; dendrimers, polymeric materials, mesoporous silica and zeolites have been also extensively utilized for the immobilization of these catalysts.⁹ However, these supports often suffer important drawbacks such as low catalyst loading and weak interactions between the support and the nanoparticles.^{10a,10d} Recent studies have demonstrated that the stability of these supported catalysts depend on the rational design of the solid scaffolds, while the efficiency is controlled by the size, morphology and the extent of the nanoparticles loading.^{10e} Thus, the interactions between the metal nanoparticles and the functional groups of the supports should be optimum to hold the particles on the surface, but not to the extent that lead to unwanted side reactions. For example, despite their high surface area and robust nature, the use of mesoporous silica, usually leads to undesired side products due to the strong interaction between loaded nanoparticles and the silanol groups on the surface.^{10b,10c} Albeit the major advances achieved in this area during the last few years,¹¹ the issues regarding sintering, leaching, stability and recyclability of supported nanoparticles remain a big concern.¹²

In these regards, the synthesis of highly stable, recyclable and equally efficient heterogeneous catalyst is mandatory. In contrast to tedious procedures reported earlier,^{2b,2g,2h,3i,4b,4c} herein, we report the successful incorporation of both Pd(0) nanoparticles and Pd(II) complex on a highly stable, crystalline and porous COF support, **TpPa-1** by a simple solution infiltration method carried out at RT (scheme 1).¹³ The most important aspect of these hybrids is their remarkable stability in water and under

harsh conditions (e.g., strong basic or acidic conditions), which remains associated with the judicious selection of the COF (**TpPa-1**) framework enriched with nitrogen and oxygen atoms. The COF skeleton imparted stability to the active metal centers and the strong interaction of loaded Pd(0) nanoparticles and Pd(II) complex with the nitrogen and oxygen atoms within the selected COF not only facilitates the catalysis in the absence of additional ligands but also provides extra strength.¹⁴ Herein, beside the synthesis of robust and stable catalyst, remarkable catalytic activities of these hybrid materials towards C–C bond formation reactions under basic conditions (i.e., Sonogashira coupling, Heck coupling) and C–H activation reactions at acidic conditions (i.e., intramolecular oxidative biaryl coupling) are also described.

Result and discussion

The presence of all characteristics peaks of **TpPa-1** in the FT-IR spectrum of **Pd(0)@TpPa-1** and **Pd(II)@TpPa-1** confirmed that, even after strong treatment with NaBH₄, the chemical environment within the COF remained intact (Figure 1a). After incorporation of Pd(0) nanoparticles and Pd(II) complex inside the **TpPa-1** matrix, the appearance of representative peaks for C=C (1580 cm⁻¹) and C–N (1251 cm⁻¹) stretching of **TpPa-1**, confirmed the metal loading without disturbing the basic COF architecture. An almost unchanged PXRD pattern for **Pd(0)@TpPa-1** with additional peaks for (111) and (200) planes appearing at 39° (2θ) and 44° (2θ) demonstrated that the loading of Pd(0) nanoparticles occurred with minimal loss of crystallinity and retention of the COF integrity (Figure 1c).^{7c} The slight broadening of the peak present at 25° (2θ) suggested increased defects in the π–π stacking of **TpPa-1** due to the incorporation of Pd(0) nanoparticles into the interlayer space within the COF

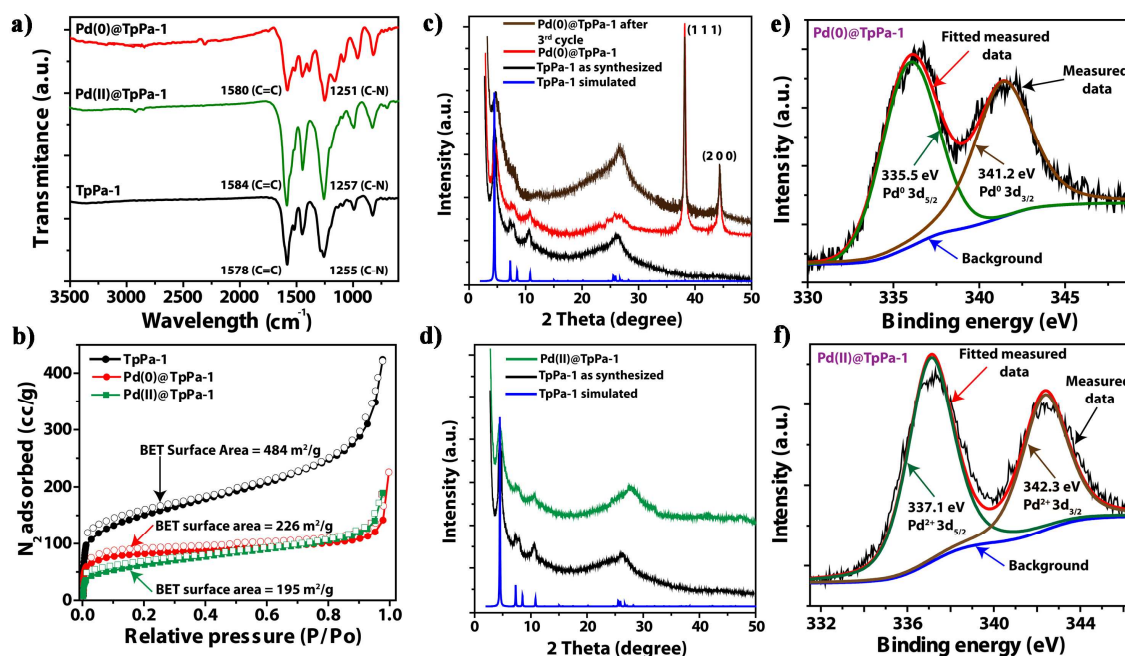


Fig. 1 Characterization of Pd(0)@TpPa-1 and Pd(II)@TpPa-1 catalysts. a) Comparison of the FT-IR spectra of Pd(0)@TpPa-1, Pd(II)@TpPa-1 and pristine TpPa-1. b) N₂ adsorption isotherms for TpPa-1, Pd(0)@TpPa-1 and Pd(II)@TpPa-1. c) PXRD profile of Pd(0)@TpPa-1 showing the characteristic peaks for (111) and (200) planes of Pd nanoparticles at 39° and 45°. Matching PXRD plots of TpPa-1, Pd(0)@TpPa-1 and Pd(0)@TpPa-1 after 3rd catalytic cycle. d) PXRD profile of Pd(II)@TpPa-1 showing matching PXRD plots for TpPa-1 and Pd(II)@TpPa-1. e) XPS spectrum of the Pd(0)@TpPa-1 in the 3d region showing typical peaks at 335.5 eV (3d_{5/2}) and 341.2 eV (3d_{3/2}) for Pd(0). f) XPS spectrum of the Pd(II)@TpPa-1 in the 3d region showing characteristic peaks at 337.1 eV (3d_{5/2}) and 342.3 eV (3d_{3/2}) for Pd(II). Black line: Measured XPS data, Red line: Measured XPS data after fitting, Green line: Pd⁰3d_{5/2} or Pd²⁺3d_{5/2}, Brown line: Pd⁰3d_{3/2}/Pd²⁺3d_{3/2}, Blue line: Background.

architecture. This phenomenon is very similar to the peak broadening observed during the exfoliation of multi-walled carbon nanotubes.^{15a} On the other side, the absence of peaks at 39° (2 θ) and 44° (2 θ) and the presence of a broad peak at 25° (2 θ) for Pd(II)@TpPa-1, underlined the exclusive loading of Pd(II) on the TpPa-1 matrix (Figure 1d). An appreciable decrease in both the N₂ adsorption and BET surface area of Pd(0)@TpPa-1 (226 m²/g) and Pd(II)@TpPa-1 (195 m²/g) in comparison to 20 pristine TpPa-1 (484 m²/g), indicates that the pore surface and interlayer spacings in the host framework are occupied by finely dispersed Pd(0) nanoparticles and Pd(II) complex located at the surface as well as inside the COF matrix (Figure 1b, ESI, Figure S7 and S12). The similar effect of the incorporation of Pd(0) and Pd(II) on the crystallite surfaces and interlayer spacings has been reflected in the micropore surface area of the hybrid, which has not experienced a dramatic change (ESI, Table S7). Further, we performed XPS measurements in order to confirm the oxidation state of the palladium loaded within the COF (ESI, Figure S8, and S13). As shown in Figure 1e, in the case of Pd(0)@TpPa-1, the 3d region showed the characteristic peaks at 335.5 eV and 341.2 eV, which could be assigned to 3d_{5/2} and 3d_{3/2} states of Pd(0), respectively. This result indicates the successful reduction step by NaBH₄. The slightly broadened peak at 25° (2 θ) reflects increased defects in the COF framework, and a positive shift of the binding energy by 0.7 eV for the N1s region indicates (in comparison to Pd-N interaction in Pd-phenanthroline complex) a strong interaction between the imine -N atoms of the framework and the incorporated metallic centers.¹⁶ Similarly, as shown in Figure 1f, the 3d region in the case of Pd(II)@TpPa-1 showed

characteristic peaks at 337.1 eV and 342.3 eV, which could be assigned to 3d_{5/2} and 3d_{3/2} states of Pd(II). However, we observed a negative shift for the binding energy in comparison with Pd(OAc)₂, probably due to the donation of electrons from the imine -N atoms of the COF matrix to the Pd(II) species (ESI, Figure S13).^{2c}

As the factors such as structure, size and morphology of the metal nanoparticles, as well as their interactions with supporting matrices influence their catalytic properties, we performed SEM, TEM and energy dispersive X-ray (EDX) analysis of both Pd(0)@TpPa-1 and Pd(II)@TpPa-1 catalysts.^{15b-15c} From the SEM images of TpPa-1 and Pd(0)@TpPa-1, it was clear that the typical flowerlike morphology of TpPa-1 was maintained in the Pd(0)@TpPa-1 after the incorporation of Pd(0) nanoparticles (ESI, Figure S2, S4 and S6). Each individual flower could be considered as the result of aggregation of a large number of petals with lengths in the micrometer scale (2±1 μ m). As shown in Figure 2a, individual petals have a sheet-like structure that could be formed as the result of π - π stacking of COF layers. High resolution and dark field TEM analyses of Pd(0)@TpPa-1 exhibited 3D distribution of Pd(0) nanoparticles (7±3 nm) into the COF matrix (Figure 2b and 2c; ESI, Figure S5). Along with these finely distributed nanoparticles, there are few nanoparticles having sizes larger than 10 nm clearly visible in the TEM analyses (Figure 4e). These nanoparticles seem to be formed by the fusion of 3-4 smaller sized nanoparticles. These Pd nanoparticles are small enough to get incorporated on top of the pores and in the interlayer spacing present in TpPa-1. However, as per calculations based on the XRD studies using Scherrer Equation,

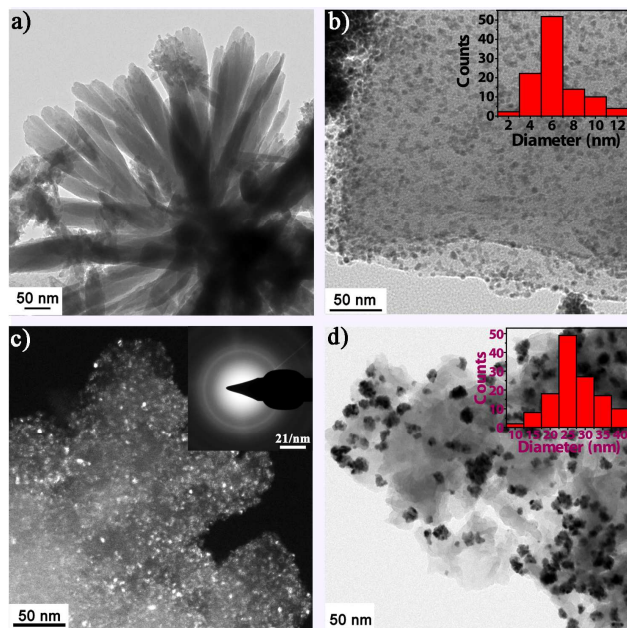


Fig. 2 (a) TEM images of pristine **TpPa-1**, **Pd(0)@TpPa-1** and **Pd(II)@TpPa-1**. a) TEM image of **TpPa-1** COF showing sheet like structures. b) Uniform distribution of 4 ± 2 nm sized Pd(0) nanoparticles on the surface of **TpPa-1** COF. Inset figure: Nanoparticles size distribution histogram. c) Dark field imaging of the **Pd(0)@TpPa-1** showing distribution of the Pd nanoparticles throughout the COF matrix. Inset figure: SAED pattern. d) Loading of Pd(II) complex on the surface of **TpPa-1** COF showing distribution of these particles at low magnification.¹⁷ Inset figure: Size distribution histogram.

size of these nanoparticles is ~ 12 nm. The probable reason for these size differences may be governed by factors like instrumental profile, solid solution in-homogeneity, micro-strain and temperature.^{15d} Also, in addition to these factors, the non-homogeneous behavior of these dispersed nanoparticles may also contribute to the overall size differences from XRD and TEM, as the bigger Pd nanoparticles formed upon agglomeration of few small sized nanoparticles usually contributes in the XRD diffraction signals. Further, the TEM analyses of **Pd(II)@TpPa-1** showed aggregation of 20 ± 10 nm sized Pd(0) nanoclusters (Figure 2d and ESI, Figure S10), which may appear due to spontaneous reduction of Pd(II) into Pd(0) as a consequence of the high energy electron beam during TEM analyses. This phenomenon in which the loaded metals first gets agglomerated and further reduced during TEM analyses has been well documented in the literature.¹⁷ EDX analyses of **Pd(0)@TpPa-1** and **Pd(II)@TpPa-1** catalysts indicated a loading of 6.4 wt.% and 10.2 wt.%, for Pd(0) and Pd(II) respectively (ESI, Figure S6 and S11). Consistent results were also obtained from the TGA traces either under air or N₂ atmosphere (ESI, Figure S25).

Considering the described unique features of the Pd(0)-doped COF, we decided to evaluate its potential catalytic properties for the copper and ligand free Sonogashira coupling reaction between aryl iodides and terminal aromatic/aliphatic alkynes under basic conditions ($\text{pH} \geq 10$).¹⁸ It is noteworthy that such process using MOF/COF supported nanoparticles without loss of crystallinity after several cycles has not been yet documented. Preliminary experiments showed that the model reaction between iodobenzene (3 mmol) and phenylacetylene (3.3 mmol) using 15

40 mg of **Pd(0)@TpPa-1** (9.62×10^{-3} mmol of Pd) as catalyst and excess of K₂CO₃ (6.6 mmol) as base proceeded smoothly in CH₃OH at 105 °C affording the desired 1,2-diphenylethyne (1,2-DPE) within 6 h in excellent isolated yield (90%). Kinetic analysis showed completion of the reaction within 6 h (Figure 45 3a). The catalytic performance shown by **Pd(0)@TpPa-1** in absence of CuI, which is considered as a potential contaminant, brings out an extra advantage towards the catalysis at environmentally friendly conditions.

At this point, we performed a series of experiments in order 50 to optimize the reaction conditions. Thus, the reaction in the absence of any base resulted in a negligible conversion (ESI, Table S1, entry 1). Among a variety of bases that showed satisfactory conversions (e.g., K₂CO₃, K₃PO₄, KOH, Et₃N, NH₄OH) (ESI, Table S1, entry 2–6), we choose to proceed with 55 K₂CO₃, because it was the easiest to handle and also afforded the highest conversion. In terms of solvent, CH₃OH afforded the desired product with the highest yield (ESI, Table S2, entry 1). Other solvent systems such as CH₃CN, toluene, *i*PrOH, or mixtures of *i*PrOH/H₂O at different v/v ratios resulted in poorer 60 yields (ESI, Table S2). Along this line, we have tested our catalyst **Pd(0)@TpPa-1** with various volume ratios of

Table 1. Sonogashira coupling between aryl iodides and aromatic/aliphatic alkynes.^a

Entry	R	R'	Conv. ^{b,f} (%)	Yield ^{c,f} (%)	TON ^d	TOF ^e (h ⁻¹)
1	H	Ph	98	90	305	51
2	CH ₃	Ph	95	89	296	49
3	OCH ₃	Ph	86	78	268	45
4	CF ₃	Ph	84	76	262	44
5	NO ₂	Ph	80	74	249	42
6	I	Ph	92	86	287	48
7	Br	Ph	68	60	187	35
8	CO ₂ H	Ph	4 ^e	–	–	–
9 ^h	H	Ph	62	58	193	32
10	H	CH ₂ OH	98	94	305	51
11	H	<i>t</i> BuSi	97	92	302	50
12	I	<i>t</i> BuSi	95	90	296	49

^a Reaction conditions: **Aryl iodide** (3 mmol), **alkyne** (3.3 mmol), **Pd(0)@TpPa-1** (15 mg, 9.62×10^{-3} mmol), 105 °C, 6 h.

^b Conversion of aryl halide calculated by GC.

^c Product isolated yield.

^d TON = turnover number (catalyst productivity).

^e TOF = turnover frequency (catalyst activity).

^f The values are the average of two independent experiments. Estimated error = 2%.

^g Conversion after 9 h.

^h Involves reaction between **bromobenzene** (1.0 mmol), **phenylacetylene** (1.05 mmol), **Pd(0)@TpPa-1** (15 mg, 9.62×10^{-3} mmol) in DMF (5 mL) in presence of K₂CO₃ (1.2 mmol), CuI (2.0 mol %) and Ph₃P (1.0 mol %) at 120 °C for 6 h.

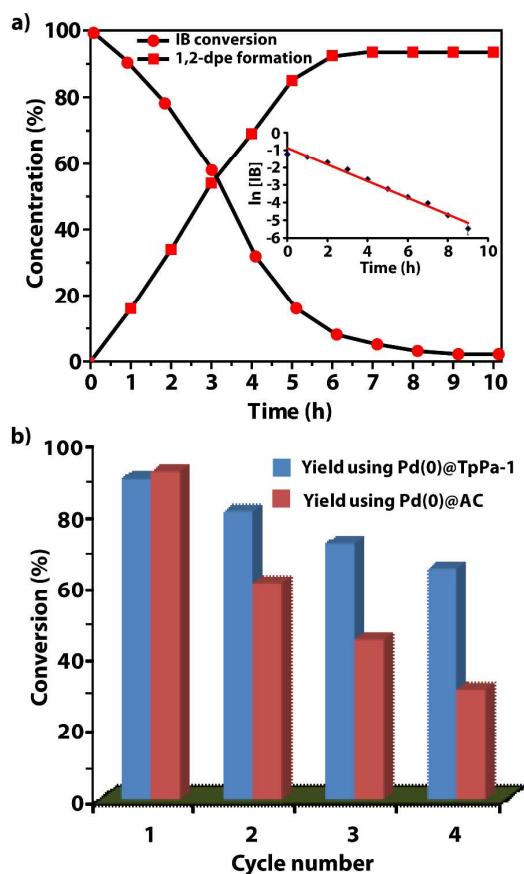


Fig. 3 Reaction kinetics and recyclability of **Pd(0)@TpPa-1** and **Pd(0)@AC** catalysts. a) Kinetics of the model Sonogashira reaction between iodobenzene (IB) and phenylacetylene. Inset figure: Plot of natural logarithm of the remained concentration of iodobenzene during reaction vs. time. $k_{\text{obs}} = 0.476 \pm 0.013 \text{ h}^{-1}$; $t_{1/2} = 1.46 \text{ h}$. b) Comparison of the recyclability studies performed for **Pd(0)@TpPa-1** and **Pd(0)@AC** catalysts for the model Sonogashira reaction.

$\text{CH}_3\text{OH}/\text{H}_2\text{O}$ and, interestingly, we observed that **Pd(0)@TpPa-1** retains its catalytic efficiency also in the presence of water. For instance, when $\text{CH}_3\text{OH}:\text{H}_2\text{O}$ (9:1, v/v) mixture was used as solvent medium, 87% of the isolated product was observed (ESI, Table S2, entry 7). The catalyst exhibited noticeable yields (71 to 25%) even when the percentage of water was increased (ESI, Table S2, entry 8–11). Lower conversions at much higher water content probably occurred due to immiscibility of the reactants in the aqueous medium. The recyclability trends observed in 100 % methanol solvent for **Pd(0)@TpPa-1** catalyst persist also in the presence of water (Figure S22). These results highlight the versatility of the COF-based catalyst in different reaction media, and are very promising within the context of green chemistry.¹⁹ Further, as expected, no product formation was observed in control experiments in the absence of **Pd(0)@TpPa-1** (ESI, Table S3, entry 11). Based on the optimized experimental conditions, we explore the substrate scope using a number of substituted aryl iodides and aliphatic/aromatic alkynes. In general, excellent conversions (> 90%) to the desired products were observed (Table 1, entry 1–3, 6), albeit slightly lower conversions were obtained for aryl iodides containing electron-withdrawing groups (Table 1, entry 4, 5, 7). Along with the aromatic alkynes, the aliphatic alkynes have also been showed excellent catalytic conversions (Table 1, entry 10, 11, 12). The

reaction of bromo and chloro substituted aryl halides (bromobenzene and chlorobenzene) with aromatic alkyne (phenyl acetylene) have been resulted into the lower yields 62 and 23 %, respectively, due to lower activation of the substrates (ESI, Table S4).^{14b} Similarly, the model reaction of 1,2-DPE synthesis by Sonogashira coupling using bromo substituted aryl halides, wherein Pd supported on activated charcoal (1 wt.%, 5 wt.%; Aldrich Chemicals) has been used as catalyst resulted into the lower yields (~ 76 %) compared to the iodo substituted aryl halides (98 %).

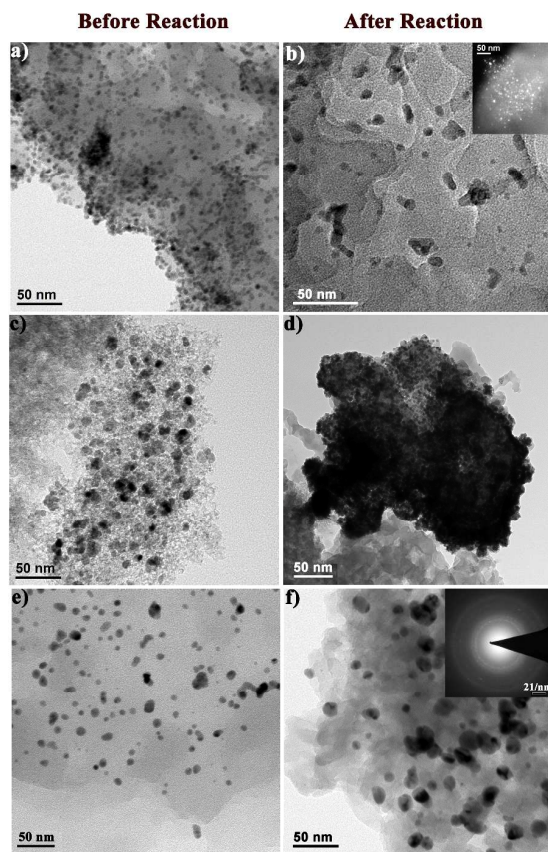


Fig. 4 Comparative TEM images. a) Freshly prepared **Pd(0)@TpPa-1** catalyst. b) **Pd(0)@TpPa-1** catalyst after 2nd cycle in the Sonogashira model reaction. Inset figure: Dark field image. c) Commercially available **Pd(0)@AC** (1 wt.%). d) **Pd(0)@AC** after 1st cycle in the Sonogashira model reaction. e) Well dispersed Pd nanoparticles observed for as synthesized **Pd(0)@TpPa-1**. f) TEM image of the **Pd(0)@TpPa-1** catalyst after 2nd cycle in the Heck model reaction. Inset figure: SAED pattern.

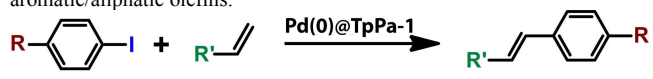
In order to confirm the heterogeneity of the catalyst, we have carried out standard leaching and mercury drop tests (ESI, Section S9, Figure S19–S21). In a typical catalyst leaching test experiment, no conversion was observed even after 12 h of reaction time (ESI, Figure S19). The results showed a tiny amount of Pd leaching under the reaction conditions (< 0.7 wt.%), which resulted insufficient for a significant catalysis. EDX analysis of the above filtrate solution revealed only a tiny amount Pd (less than 0.7 wt.%) in the solution (ESI, Figure S20). This experiment suggests strong interaction of Pd(0) nanoparticles with **TpPa-1** for **Pd(0)@TpPa-1**, without Pd leaching and proves that the heterogeneity of the catalyst remains intact in standard

catalytic conditions. Moreover, catalytic experiments in the presence of a drop of metallic mercury resulted in negligible product formation (< 1%), because mercury poisons the surface of heterogeneous catalysts and thus reduces its catalytic activity (ESI, Figure S21). The facile adsorption and desorption of small reactant/product molecules on the **Pd(0)@TpPa-1** was validated by carbon mass balance of the reaction. The constant % of carbon observed in both the cases of pristine and used **Pd(0)@TpPa-1** from CHN analysis confirmed the adsorption of small molecules onto the 2D catalyst is followed by facile desorption (ESI, Section S10).

As an important aspect of heterogeneous catalysis, we further studied the recyclability of the catalyst for a model Sonogashira reaction. In spite of a gradual catalyst deactivation (Figure 3b), the results showed a superior recyclability of **Pd(0)@TpPa-1** in comparison to **Pd(0)@AC** catalyst (1, 5 and 10 wt.%, Aldrich Chemicals) up to four cycles, probably due to stable and less sintered **Pd(0)@TpPa-1** through the catalytic cycles (Figure 4a-4d, ESI, Table S5). Although **Pd(0)@TpPa-1** showed superior activity for the Sonogashira coupling reaction than commercially available **Pd(0)@AC**, it was acknowledged that conversion of substrate decreased almost at the same rate for both catalysts. Indeed, TEM images of the recovered catalyst showed slightly sintered Pd nanoparticles after the 2nd cycle (Figure 4b, ESI, Figure S24), whereas in the case of **Pd(0)@AC** the nanoparticles sintered after the 1st cycle (Figure 4d, ESI, Table S6). The sintering behavior of reused **Pd(0)@TpPa-1** catalyst is also in concordance with the crystalline evolution observed by PXRD (vide supra).

The results obtained with the Sonogashira coupling motivated us to evaluate other C–C bond-forming reactions also. In this sense, we were delighted to observe that, **Pd(0)@TpPa-1** also resulted very efficient for the Heck coupling reaction between a variety of aryl iodides and aliphatic/aromatic olefins under similar conditions than those used for the Sonogashira coupling (Table 2, Figure 5a). Preliminary kinetic studies comprised the

Table 2. Heck coupling reaction between aryl iodides and aromatic/aliphatic olefins.^a



Entry	R	R'	Conv. ^{b,f} (%)	Yield ^{c,f} (%)	TON ^d	TOF ^e (h ⁻¹)
1	H	Ph	95	92	312	49
2	CH ₃	Ph	92	88	293	48
3	OCH ₃	Ph	84	80	275	44
4	NO ₂	Ph	81	77	259	42
5	I	Ph	90	85	284	47
6	N	Ph	96	91	299	50
7	H	CH ₂ OH	99	95	308	51
8	H	<i>t</i> BuOCO	98	93	305	51

^a Reaction conditions: **Iodobenzene** (3 mmol), **olefin** (3.3 mmol), **Pd(0)@TpPa-1** (15 mg, 9.62×10^{-3} mmol of Pd), 105 °C, 6 h.

^b Conversion of aryl halide calculated by GC.

^c Product isolated yield.

^d TON = turnover number (catalyst productivity).

^e TOF = turnover frequency (catalyst activity).

^f The values are the average of two independent experiments. Estimated error = 2%.

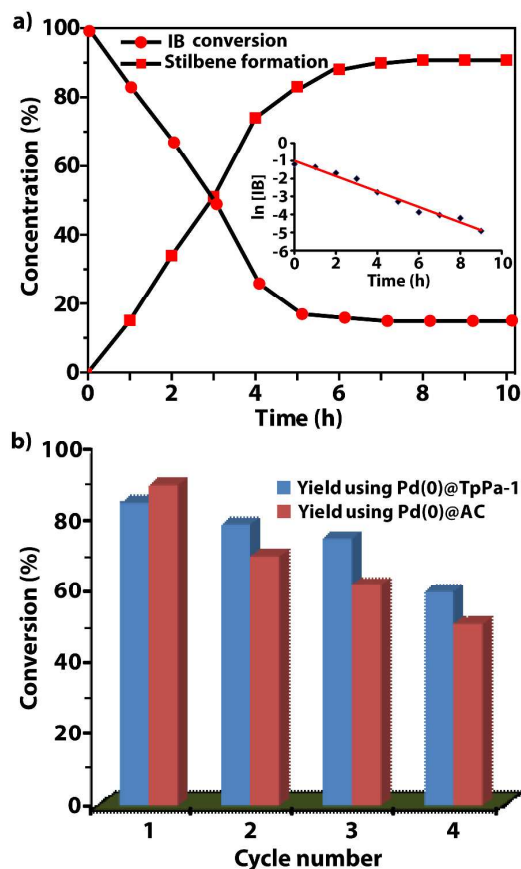
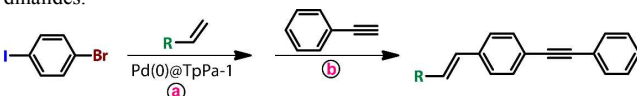


Fig. 5 Reaction kinetics and recyclability of **Pd(0)@TpPa-1** and **Pd(0)@AC** catalysts. a) Kinetics of the model Heck reaction between iodobenzene and styrene. Inset figure: Plot of natural logarithm of the remained concentration of iodobenzene during reaction vs. time. $k_{\text{obs}} = 0.430 \pm 0.004 \text{ h}^{-1}$; $t_{1/2} = 1.61 \text{ h}$. b) Comparison of the recyclability studies performed for **Pd(0)@TpPa-1** and **Pd(0)@AC** catalysts for the model Heck reaction.

entire reaction region between 0 % and 100 % conversion, in which no byproducts were detected. In general, average catalyst productivity and activity were identified in both Sonogashira and Heck reactions (TON ~ 250-300; TOF ~ 40-50 h⁻¹). Each experiment was performed at least in duplicate and average conversions were used for kinetics calculations. Under the reported conditions, both model reactions showed apparent first-order behavior (squared linear correlation coefficient, $R^2 = 0.98$), consistent with a zero-order dependence on phenylacetylene and styrene, respectively (inset plots in Figures 3a and 5a). A plausible explanation for the observed experimental rate law under our conditions may involve the oxidative addition of iodobenzene to the catalyst as the rate-determining step, in such a way that further capture of the corresponding metallo-intermediate by phenylacetylene or styrene is immediate with a consequent rapid formation of the final product. Comprehensive mechanistic studies along this line involving **Pd(0)@TpPa-1** catalyst are a subject matter in our laboratories. Similarly, reasonably good recyclability of the catalyst up to four cycles and

superior performance in comparison to **Pd(0)@AC** was observed for the Heck reaction (Figure 5b, Figure 4c–4f, ESI, Table S6).

Table 3. One-pot sequential Heck/Sonogashira coupling reactions of aryl dihalides.^a



Entry	R	Conv. ^b (%)	Yield ^b (%)	TON	TOF(h ⁻¹)
1	Ph	85	62	66	11
2	<i>t</i> BuOCO	94	85	73	12

^a Reaction conditions: **Step a:** Aryl dihalide (1.0 mmol), Olefin (1.05 mmol), DMF (7 mL), NaOAc (1.2 mmol), **Pd(0)@TpPa-1** (20 mg, 1.28×10^{-2} mmol of Pd), 120 °C, 2 h. **Step b:** Phenyl acetylene (1.5 mmol), CsCO₃ (1.2 mmol), CuI (1.5 mol %), PPh₃ (1.0 mol %), 105 °C, 4 h.

^b The values are the average of two independent experiments. Estimated error = 2 %.

After the successful utilization of **Pd(0)@TpPa-1** for Heck and Sonogashira coupling reactions, the same methodology has been extended for the one-pot sequential Heck/Sonogashira coupling reaction for the synthesis of enynes.²⁰ The Heck reaction of aromatic dihalide (i.e., 1-bromo-4-iodobenzene) with aliphatic or aromatic olefins in presence of **Pd(0)@TpPa-1** was followed with Sonogashira reaction using phenyl acetylene. After completion of Heck reaction under the standard conditions, the temperature of reaction mixture was reduced to RT and to the same mixture phenylacetylene, CsCO₃, PPh₃ and CuI were subsequently added to complete the further reaction. This one-pot Heck/Sonogashira coupling reaction afforded the respective (alkynyl)(alkenyl)arenes in good yields for both aromatic as well as aliphatic olefins as shown in Table 3. The successful completion of this process highlights the usability of the catalyst for the regioselective formation of two C–C bonds in one-pot.

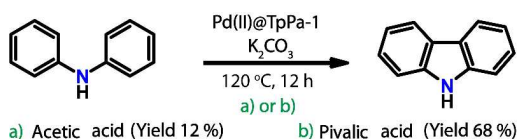


Fig. 6 Intramolecular oxidative biaryl synthesis catalyzed by **Pd(II)@TpPa-1**.

Finally, given the superior stability of the COF matrix in a wide range of pH, we also tested as a proof of concept the catalytic potential of **Pd(II)@TpPa-1** for C–H activation reaction under acidic conditions. The results demonstrated that 3 mol% of **Pd(II)@TpPa-1** was enough to catalyze the intramolecular oxidative coupling of diphenylamine under air to afford the corresponding 9*H*-carbazole. As observed with other catalysts,¹⁴ the product yield drastically increased when the reaction was carried out in pivalic acid as solvent in comparison to other acid such as acetic acid (Figure 6 and ESI, Section S9).

Conclusions

The foregoing results demonstrate that Pd(0) nanoparticles and Pd(II) complex can be immobilized into a highly stable, crystalline and porous COF, by a simple solution infiltration method followed by NaBH₄ reduction. The remarkable stability and crystalline nature of the COF matrix is maintained upon Pd

doping, which makes them suitable candidates as heterogeneous catalysts for both C–C coupling and C–H activation reactions. Specifically, the described supported and highly dispersed Pd(0) nanoparticles exhibited excellent catalytic activity towards Cu free Sonogashira and Heck coupling reactions under basic conditions, and with superior performance than the observed using commercially available Pd immobilized on activated charcoal. **Pd(0)@TpPa-1** catalyst was also efficient in one-pot sequential Heck/Sonogashira reactions. Moreover, the precursor Pd(II)-doped COF displayed competitive activity for the intramolecular oxidative biaryl synthesis under acidic conditions. The robustness and the green character of both catalyst was evidenced by their preservation under the wide-range of reaction conditions tested (i.e., organic, aqueous, acidic and basic media), showing negligible metal leaching, non-sintering behavior, and good recyclability. To the best of our knowledge, this is the first report dealing with the separate incorporation of Pd(0) nanoparticles and Pd(II) complex on the same COF support, and their use as heterogeneous catalysts in both C–C coupling and C–H activation reactions, respectively.

Experimental Section

The COF, **TpPa-1**, used for the loading of Pd(0) and Pd(II) nanoparticles was synthesized according to the procedure reported in our recent communication.¹² The general procedures were followed for the Sonogashira, Heck, sequential one pot Heck/Sonogashira coupling reactions and intramolecular oxidative biaryl synthesis reaction. All the products obtained from aforementioned reactions are known and described in the literature and spectroscopic data were identical to those reported (ESI, Section S5-S9).

Synthesis of **Pd(0)@TpPa-1** and **Pd(II)@TpPa-1**:

In a typical synthesis of **Pd(0)@TpPa-1**, pre-synthesized and activated **TpPa-1** (100 mg) was dispersed in 5 mL of MeOH under ambient conditions, to which a MeOH solution (2 mL) containing Na₂PdCl₄ (20 mg, 0.07 mmol) was added dropwise under vigorous stirring. The mixture was evaporated until it became mushy. To this solution, 4 mL of MeOH was subsequently added into the slurry, followed by a solution (3 mL) of NaBH₄ (2 M in MeOH) under vigorous stirring. After 30 min, the residue was recovered by filtration and thoroughly washed several times with MeOH (3 × 10 mL) to remove any impurity (Scheme 1 and ESI, Section S3). The so-prepared sample of **Pd(0)@TpPa-1** was further dried in a vacuum drying oven at 50 °C. Similarly, the synthesis of **Pd(II)@TpPa-1** was performed using Pd(OAc)₂ as metal precursor. In a typical synthesis, activated **TpPa-1** (100 mg) were impregnated with Pd(OAc)₂ (20 mg, 0.093 mmol) via sonication using an ultrasonic bath for 30 min and, followed by vigorously stirring for 1 h at RT (Scheme 1). The obtained residue was filtered and washed using aliquots of MeOH (3 × 10 mL) to yield **Pd(II)@TpPa-1**. The so-prepared sample of **Pd(II)@TpPa-1** was further dried in a vacuum drying oven at 50 °C (ESI, Section S4).

Acknowledgment

PP acknowledges CSIR for a Senior Research Fellowship (SRF). RB thanks Dr. A. T. Biju and Dr. D. Srinivasa Reddy, CSIR-National Chemical Laboratory, Pune, India, for useful

discussions. Financial assistance from CSIR (CSC0122 and CSC0102) and DST (SB/S1/IC-32/2013) is acknowledged.

Notes and references

^a Physical/Materials Chemistry Division, CSIR-National Chemical Laboratory, Dr. Homi Bhabha Road, Pune-411008, India.

E-mail: r.banerjee@ncl.res.in

^b International Centre for Material Science, Jawaharlal Nehru Centre for Advanced Scientific Research, Bangalore 560064, India.

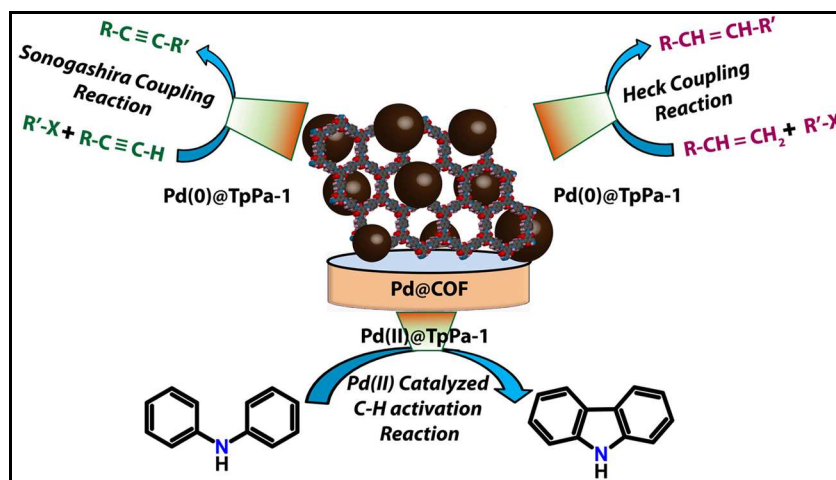
^c Institut für Organische Chemie, Universität Regensburg, Universitätsstr. 31, 93040 Regensburg, Germany.

† Electronic Supplementary Information (ESI) available: [Detailed experimental procedures, characterization data, CIF files, additional figures and tables]. See DOI: 10.1039/b000000x/

- (a) K. Sakaushi, E. Hosono, G. Nickerl, T. Gemming, H. Zhou, S. Kaskel, J. Eckert, *Nat. Commun.* 2013, **4**, 1485; (b) M. Dogru and T. Bein, *ChemComm*, 2013, DOI: 10.1039/C3CC46767H. (c) J. W. Colson and W. R. Dichtel, *Nat. Chem.* 2013, **5**, 453-465; (d) X. Feng, X. Ding, D. Jiang, *Chem. Soc. Rev.* 2012, **41**, 6010-6022; (e) C. J. Doonan, D. J. Tranchemontagne, T. G. Glover, J. R. Hunt and O. M. Yaghi, *Nat. Chem.*, 2010, **2**, 235-238. (f) Y. Xu, S. Jin, H. Xu, A. Nagai and D. Jiang, *Chem. Soc. Rev.*, 2013, **42**, 8012-8031.
- (a) R. Palkovits, M. Antonietti, P. Kuhn, A. Thomas and F. Schuth, *Angew. Chem., Int. Ed.* 2009, **48**, 6909-6912. (b) C. E. Chan-Thaw, A. Villa, P. Katekomol, D. Su, A. Thomas and L. Prati, *Nano Lett.* 2010, **10**, 537-541. (c) S.-Y. Ding, J. Gao, Q. Wang, Y. Zhang, W.-G. Song, C.-Y. Su and W. Wang, *J. Am. Chem. Soc.* 2011, **133**, 19816-19822. (d) S. B. Kalidindi, K. Yussenko and R. A. Fischer, *Chem. Commun.* 2011, **47**, 8506-8508. (e) C. E. Chan-Thaw, A. Villa, L. Prati and A. Thomas, *Chem. Eur. J.* 2011, **17**, 1052-1057. (f) P. Zhang, Z. Weng, J. Guo and C. Wang, *Chem. Mater.* 2011, **23**, 5243-5249. (g) S. B. Kalidindi, H. Oh, M. Hirscher, D. Esken, C. Wiktor, S. Turner, G. V. Tendeloo and R. A. Fischer, *Chem. Eur. J.* 2012, **18**, 10848-10856. (h) Y. Zhou, Z. Xiang, D. Cao and C.-J. Liu, *Chem. Commun.* 2013, **49**, 5633-5635.
- (a) Y. K. Hwang, D.-Y. Hong, J.-S. Chang, S. H. Jhung, Y.-K. Seo, J. Kim, A. Vimont, M. Daturi, C. Serre and G. Férey, *Angew. Chem., Int. Ed.* 2008, **47**, 4144-4148. (b) X.-L. Yang, M.-H. Xie, C. Zou, Y. He, B. Chen, M. O'Keeffe, C.-D. Wu, *J. Am. Chem. Soc.*, 2012, **134**, 10638-10645. (c) C. Zlotea, R. Campesi, F. Cuevas, E. Leroy, P. Dibandjo, C. Volkringer, T. Loiseau, G. Férey and M. Latroche, *J. Am. Chem. Soc.* 2010, **132**, 2991-2997. (d) S. Gao, N. Zhao, M. Shu and S. Che, *Appl. Catal., A* 2010, **388**, 196-201. (e) T.-H. Park, A. J. Hickman, K. Koh, S. Martin, A. G. Wong-Foy, M. S. Sanford and A. J. Matzger, *J. Am. Chem. Soc.* 2011, **133**, 20138-20141. (f) H. L. Jiang, T.; Akita, T. Ishida, M. Haruta and Q. Xu, *J. Am. Chem. Soc.* 2011, **133**, 1304-1306. (g) C. Wang, K. E. deKrafft and W. Lin, *J. Am. Chem. Soc.* 2012, **134**, 7211-7214. (h) C.-H. Kuo, Y. Tang, L.-Y. Chou, B. T. Sneed, C. N. Brodsky, Z. Zhao and C.-K. Tsung, *J. Am. Chem. Soc.* 2012, **134**, 14345-14348. (i) J. Long, H. Liu, S. Wu, S. Liao and Y. Li, *ACS Catal.* 2013, **3**, 647-654. (j) M. Yadav and Q. Xu, *Chem. Commun.* 2013, **49**, 3327-3329. (k) H.-L. Jiang, B. Liu, T. Akita, M. Haruta, H. Sakurai and Q. Xu, *J. Am. Chem. Soc.* 2009, **131**, 11302-11303.
- (a) S. Proch, J. Herrmannsdörfer, R. Kempe, C. Kern, A. Jess, L. Seyfarth and L. Senker, *Chem. Eur. J.* 2008, **14**, 8204-8212. (b) T. Ishida, M. Nagaoka, T. Akita and M. Haruta, *Chem. Eur. J.* 2008, **14**, 8456-8460. (c) A. Aijaz, A. Karkamkar, Y. J. Choi, N. Tsumori, E. Rönnebro, T. Autrey, H. Shioyama and Q. Xu, *J. Am. Chem. Soc.* 2012, **134**, 13926-13929.
- (a) B. H. Lipshultz and S. Sengupta, *Org. React.* 1992, **41**, 135-631. (b) N. Miyaoura and A. Suzuki, *Chem. Rev.* 1995, **95**, 2457-2483. (c) *Metal-catalyzed Cross-coupling Reactions* (Eds.: F. Diederich and P. J. Stang), WILEY-VCH, Weinheim, 1998. (c) *Transition Metals for Organic Synthesis*, Vol. 1, chap. 2.10, (Eds.: M. Beller and C. Bolm), WILEY-VCH, Weinheim, 1998, 158-183. (d) D. J. Cárdenas, *Angew. Chem., Int. Ed.* 1999, **38**, 3018-3020. (e) X. Chen, K. M. Engle, D.-H. Wang and J.-Q. Yu, *Angew. Chem., Int. Ed.* 2009, **48**, 5094-5115.
- (a) K. J. Sonogashira, *Organomet. Chem.* 2002, **653**, 46-49. (b) *Palladium-Catalyzed Coupling Reactions: Practical Aspects and Future Developments*, (Eds.: Á. Molnár), John Wiley & Sons, 2013. (c) W. Kleist, S. Pröckl and K. Köhler, *Catal. Lett.* 2008, **128**, 197-200. (d) M. T. Reetz and E. Westermann, *Angew. Chem., Int. Ed.* 2000, **39**, 165-168.
- (a) B. Åkermark, L. Ebersson, E. Jonsson and E. Pettersson, *J. Org. Chem.* 1975, **40**, 1365-1367. (b) N. T. S. Phan, M. Van Der Sluys and C. W. Jones, *Adv. Synth. Catal.* 2006, **348**, 609-679. (c) W. Niu, L. Zhang, G. Xu, *ACS Nano* 2010, **4**, 1987-1996.
- (a) A. Fukuoka and P. L. Dhepe, *Chem. Rev.* 2009, **9**, 224-235. (b) S. Schauermaier, N. Nilius, S. Shaikhutdinov and H.-J. Freund, *Acc. Chem. Res.*, 2013, **46**, 1673-1681. (c) L. L. Chng, N. Erathodiyil and J. Y. Ying, *Acc. Chem. Res.* 2013, **46**, 1825-1837.
- (a) R. L. Augustine and S. T. O'Leary, *J. Mol. Catal.* 1992, **72**, 229-242. (b) H. Sakurai, T. Tsukuda and T. Hirao, *J. Org. Chem.* 2002, **67**, 2721-2722. (c) M. Dams, L. Drijkoningen, B. Pauwels, G. Van Tendeloo, D. E. De Vos and P. A. Jacobs, *J. Catal.* 2002, **209**, 225-236. (d) P. Raveendran, J. Fu and S. L. Wallen, *J. Am. Chem. Soc.* 2003, **125**, 13940-13941. (e) R. B. Bedford, U. G. Singh, R. I. Walton, R. T. Williams and S. A. Davis, *Chem. Mater.* 2005, **17**, 701-707. (f) N. Erathodiyil, S. Ooi, A. M. Seayad, Y. Han, S. S. Lee and J. Y. Ying, *Chem. Eur. J.* 2008, **14**, 3118-3125. (g) H. C. Zeng, *Acc. Chem. Res.* 2013, **46**, 226-235. (h) C. Janiak, *Z. Naturforsch.* 2013, **68b**, 1059-1089. (i) M. Kralik and A. Biffis, *J. Mol. Catal. A: Chem.* 2001, **177**, 113-138.
- (a) A. Corma, *Chem. Rev.* 1997, **97**, 2373-2419. (b) Y. Zhang, L. Zhao, S. S. Lee and J. Y. Ying, *Adv. Synth. Catal.* 2006, **348**, 2027-2032. (c) Y. Zhang, L. Zhao, P. K. Patra and J. Y. Ying, *Adv. Synth. Catal.* 2008, **350**, 662-666. (d) J. Lu and P. H. Toy, *Chem. Rev.* 2009, **109**, 815-838. (e) U. Diaz, T. Garcia, A. Velty and A. Corma, *Chem. Eur. J.* 2012, **18**, 8659-8672.
- (a) A. Dhakshinamoorthy and H. Garcia, *Chem. Soc. Rev.* 2012, **41**, 5262-5284. (b) Y. Zhang and S. N. Riduan, *Chem. Soc. Rev.* 2012, **41**, 2083-2094. (c) H. R. Moon, D.-W. Lim and M. P. Suh, *Chem. Soc. Rev.* 2013, **42**, 1807-1824. (d) C. Janiak and J. K. Vieth, *New J. Chem.*, 2010, **34**, 2366-2388. (e) C. Janiak, *Dalton Trans.*, 2003, 2781-2804. (f) E. J. Mittemeijer and U. Welzel, *Petroleum Chemistry*, 2010, **50**, 167-180. (g) S.-Y. Ding and W. Wang, *Chem. Soc. Rev.*, 2013, **42**, 548-568.
- (a) P. Forzatti and L. Lietti, *Catal. Today* 1999, **52**, 165-181. (b) P. Albers, J. Pietsch and S. F. Parker, *J. Mol. Catal. A: Chem.*, 2001, **173**, 275-286.
- (a) S. Kandambeth, A. Mallick, B. Lukose, M. V. Mane, T. Heine and R. Banerjee, *J. Am. Chem. Soc.* 2012, **134**, 19524-19527. (b) B. P. Biswal, S. Chandra, S. Kandambeth, B. Lukose, T. Heine and R. Banerjee, *J. Am. Chem. Soc.* 2013, **135**, 5328-5331.
- (a) K. C. Nicolaou, P. G. Bulger and D. Sarlah, *Angew. Chem., Int. Ed.* 2005, **44**, 4442-4489. (b) R. Chinchilla and C. Nájera, *Chem. Rev.* 2007, **107**, 874-922. (c) B. Liégault, D. Lee, M. P. Huestis, D. R. Stuart and K. Fagnou, *J. Org. Chem.* 2008, **73**, 5022-5028.
- (a) A. G. Cano-Marquez, F. J. Rodriguez-Macias, J. Campos-Delgado, C. G. Espinosa-Gonzalez, F. Tristan-Lopez, D. Ramirez-Gonzalez, D. A. Cullen, D. J. Smith, M. Terrones and Y. I. Vega-Cantu, *Nano Lett.* 2009, **9**, 1527-1533. (b) A. T. Bell, *Science* 2003, **299**, 1688; (c) M. S. Chen and D. W. Goodman, *Catal. Today*, 2006, **111**, 22. (d) Eric J. Mittemeijer and U. Z. Welzel, *Kristallogr.* 2008, **223**, 552-560.
- (a) Z. Jin, D. Nackashi, W. Lu, C. Kittrell and J. M. Tour, *Chem. Mater.* 2010, **22**, 5695-5699. (b) R. Wojcieszak, M. J. Genet, P. Eloy, P. Ruiz and E. M. Gaigneaux, *J. Phys. Chem. C* 2010, **114**, 16677-16684. (c) S. Akbayrak, M. Kayab, M. Volkan and S. Özkaz, *Appl. Catal., B*, 2014, **147**, 387-393. (d) Y. Zhang, X. He, J. Ouyang and H. Yang, *Sci. Rep.*, 2013, **3**, 2948. (e) X. Huang, Y. Wang, X. Liao and B. Shi, *Chem. Commun.*, 2009, 4687-4689.
- As demonstrated by XPS analysis (ESI, Figure S16) oxidation state of the palladium incorporated into the **TpPa-I** matrix is +2. However, the black clusters of 20±10 nm observed in the TEM images of **Pd(II)@TpPa-I** (Figure 2d and S10) can be related to the

- Pd(0) nanoparticles formed upon the electron-beam induced reduction of the original Pd(II) species during the TEM measurements. See for example: (a) T. J. Stark, T. M. Mayer, D. P. Griffis and P. E. Russell, *J. Vac. Sci. Technol. B* 1991, **9**, 3475-3478.
- 5 (b) R. Wahl, M. Mertig, J. Raff, S. Selenska-Pobell and W. Pompe, *Adv. Mater.* 2001, **13**, 736-740. (c) H. R. Moon, J. H. Kim and M. P. Suh, *Angew. Chem., Int. Ed.* 2005, **44**, 1261-1265. (d) R. J. T. Houk, B. W. Jacobs, F. E. Gabaly, N. N. Chang, A. A. Talin, D. D. Graham, S. D. House, I. M. Robertson and M. D. Allendorf, *Nano Lett.* 2009, **9**, 3413-3418.
- 10 18. (a) J.-Z. Jiang and C. Cai, *J. Colloid Interface Sci.* 2007, **307**, 300-303. (b) M. Bakherad, A. Keivanloo, B. Bahramian and S. Mihanparast, *Tetrahedron Lett.* 2009, **50**, 6418-6420. (c) D. Saha, R. Dey and B. C. Ranu, *Eur. J. Org. Chem.* 2010, 6067-6071.
- 15 19. M. Bakherad, *Appl. Organometal. Chem.* 2013, **27**, 125-140.
20. (a) X. Zhang, A. Liu and W. Chen, *Org. Lett.* 2008, **10**, 3849-3852. (b) A. Jiblaoui, C. Baudequin, V. Chaleix, G. Ducourthial, F. Louradour, Y. Ramonden, V. Sol and S. Leroy-Lhez, *Tetrahedron*, 2013, **69**, 5098-5103.

TABLE OF CONTENT GRAPHIC



Highly stable COF supported Pd(0) and Pd(II) nanoparticles (i.e. **Pd(0)@Tppa-1**, **Pd(II)@TpPa-1**) have been synthesized. **Pd(0)@TpPa-1** serve as a robust and efficient heterogeneous catalyst for copper free Sonogashira and Heck coupling reactions under basic conditions, whereas **Pd(II)@TpPa-1** satisfactorily catalyzes intramolecular oxidative biaryl synthesis under acidic conditions.